Thermal Stability and Isomerization Mechanism of *exo*-Tetrahydrodicyclopentadiene: Experimental Study and Molecular Modeling

Sun Hee Park,[†] Cheong Hoon Kwon,[†] Joongyeon Kim,[†] Byung-Hee Chun,[†] Jeong Won Kang,[†] Jeong Sik Han,[‡] Byung Hun Jeong,[‡] and Sung Hyun Kim*[,†]

Department of Chemical & Biological Engineering, Korea University, 1 Anam-Dong, Sungbuk-Ku, Seoul 136-701, Korea, and Agency for Defense Development, Jochiwongil 462, Yuseong, Daejon, Korea

Thermal stability and the primary initiation mechanism of *exo*-tetrahydrodicyclopentadiene (*exo*-THDCP, $C_{10}H_{16}$) were investigated in a batch-type reactor. The catalytic role of the stainless steel inside the reactor was eliminated by inserting a quartz flask. *exo*-THDCP decomposed at temperatures over 623 K and 1-cyclopentylcyclopentene (1-CPCP, $C_{10}H_{16}$) and 4-methyl-2,3,4,5,6,7-hexahydro-1*H*-indene (4-MHI, $C_{10}H_{16}$) were the primary decomposition products of *exo*-THDCP. C_{10} hydrocarbons were determined to be the major products. The amount of C_5-C_7 hydrocarbons, such as cyclopentene, benzene, and toluene, were relatively small. We performed the molecular modeling (MM) on some of the compounds, including 1-CPCP and 4-MHI produced from *exo*-THDCP to evaluate the activation energy and molecular structure of the intermediates. The experimental and MM results showed that 1-CPCP and 4-MHI were independently formed from *exo*-THDCP. The experimental results closely corresponded with the MM result; the products that were only minimally produced after the reaction had qualitatively higher activation energies than the other products.

1. Introduction

exo-THDCP, also called *exo*-tricyclo[5.2.1.$0^{2,6}$]decane, is a synthetic liquid fuel and is used in pulse supersonic-combustion ramjets and pulse detonation engines (PDE) due to its high-energy density.[1,2] *exo*-THDCP has attracted significant attention due to its cooling ability and high thermal stability. It has the ability to absorb aerodynamic heat, which leads to coking by decomposition of the fuel, and this process causes problems with the operating system. Therefore, a lot of studies have examined the characteristics of thermal decomposition and the decomposition mechanism of *exo*-THDCP with experiment and molecular modeling.[1−10]

Several experimental studies on *exo*-THDCP provided evidence of low-molecular-weight decomposition products less than C_6 hydrocarbons and important information on the decomposition kinetics.[1−5,7−9] In these studies, methane, ethylene, propylene, benzene, cyclopentene, propene, ethylene, acetylene, 1,3-butadiene, and cyclopentadiene were measured as the decomposition products of *exo*-THDCP and pre-exponential factor, activation energy, and overall reaction order for thermal cracking of *exo*-THDCP were evaluated. However, the initiation decomposition products of *exo*-THDCP have not yet been experimentally revealed and the decomposition mechanism of *exo*-THDCP has only been schematically suggested.

To analyze the decomposition mechanism of *exo*-THDCP, computer modeling simulations[11−15] based on quantum mechanical calculations were also used. Herbinet et al. studied the thermal decomposition of *exo*-THDCP in a jet-stirred reactor over a temperature range of 848 to 933 K at atmospheric pressure and developed a primary mechanism such as the possible initiation steps and propagation reactions.[6] Chenoweth et al. performed molecular dynamics (MD) simulations for the decomposition of *exo*-THDCP by employing the ReaxFF reactive force field and found that either ethylene plus C_8 hydrocarbon or two C_5 hydrocarbons were the primary initiation products of *exo*-THDCP.[10] The information provided by these two simulation studies on *exo*-THDCP decomposition was important for a better understanding of this process. However, it was still insufficient in explaining the details of the decomposition mechanism of *exo*-THDCP in terms of the primary initiation of *exo*-THDCP. Therefore, we performed molecular modeling to analyze decomposition mechanism of *exo*-THDCP with a decomposition pathway, reaction intermediate (transient state) and activation energy.

In this study, experiments were conducted to investigate the thermal stability of *exo*-THDCP including the decomposition temperature and primary decomposition products. In addition, molecular modeling studies were performed to analyze the mechanism of *exo*-THDCP decomposition in terms of the initiation intermediate of *exo*-THDCP and activation energy. Finally, we compared the experimental results with the molecular modeling results of the decomposition mechanism of *exo*-THDCP.

2. Experiments

Thermal decomposition of *exo*-THDCP was carried out in a 160 mL batch-type reactor. A quartz flask was inserted inside the reactor made of stainless steel to remove the catalytic role of stainless steel. An electrical heating jacket was used to heat up the reactor. The reactor was purged with N_2 for 5 min to eliminate any effects of O_2 after liquid *exo*-THDCP (*exo*-THDCP, 97.878%; *trans*-decalin, 0.494%; adamantane, 0.611%; *endo*-THDCP, 1.017%) was injected into the reactor. The unit (%) of the composition iswas mol % because it was measured by GC/MSD. Since the critical pressure (P_c) of *exo*-THDCP was below 38 bar,[16] the pressure in the reactor was maintained at 45 bar to ensure that the reaction remained in the liquid phase during the reaction. Experiments were carried out for 10 h at temperatures ranging from 583 to 683 K, which were all below the critical temperature (T_c) (701 K) of *exo*-THDCP. The liquid product was sampled after the reaction and the reactor was cooled to room temperature to prevent low-molecular-weight

* Corresponding author. Tel.: +82-02-3290-3297. Fax: +82-02-926-6102. E-mail address: kimsh@korea.ac.kr.
[†] Korea University.
[‡] Agency for Defense Development.

10.1021/ie100065m
Published on Web 08/18/2010

Table 1. Composition of Reactants and Products after Thermal Decomposition of *exo*-THDCP under N_2 at 45 bar, 10 h from 608 to 683 K

compound name	MF[b]	603 K	623 K	643 K	663 K	683 K
cyclopentene	C_5H_8			0.080	0.222	0.284
1-methylcyclopentene	C_6H_{10}					0.035
ethylcyclopentane	C_7H_{14}					0.034
1-ethylcyclopentene	C_7H_{12}				0.049	0.120
methylbenzene	C_7H_8					0.041
ethylidenecyclopentane	C_7H_{12}					0.041
propylcyclopentane	C_8H_{16}					0.038
1,2,3,3a,4,6a-hexahydropentalene	C_8H_{12}			0.044	0.115	0.140
cis-octahydropentalene	C_8H_{14}					0.087
2,3,4,5,6,7-hexahydro-1*H*-indene	C_9H_{14}				0.048	0.101
3a,4,5,6,7,7a-hexahydro-4,7-methanoindene	$C_{10}H_{14}$			0.137	0.449	0.786
trans-decalin[a]	$C_{10}H_{18}$	0.494	0.508	0.752	0.973	1.051
exo-THDCP[a]	$C_{10}H_{16}$	97.878	97.432	93.386	84.395	72.145
4-methyl-2,3,4,5,6,7-hexahydro-1*H*-indene	$C_{10}H_{16}$		0.058	0.380	1.215	1.698
2,2-dimethyl-5-methylenebicyclo[2.2.1]heptane	$C_{10}H_{16}$			0.070	0.107	0.111
1,1′-bicyclopentyl	$C_{10}H_{18}$			0.092	0.381	0.976
adamantane[a]	$C_{10}H_{16}$	0.611	0.646	0.852	0.868	0.880
endo-THDCP[a]	$C_{10}H_{16}$	1.017	1.275	2.096	3.019	3.646
1-cyclopentylcyclopentene	$C_{10}H_{16}$		0.081	0.520	1.492	2.311
tricyclo[5.2.1.0(4,8)]decane	$C_{10}H_{16}$					0.071
Tricyclo[4.2.1.1(2,5)]decane	$C_{10}H_{16}$					0.049
tricyclo[4.4.0.0(2,8)]decane	$C_{10}H_{16}$				0.071	0.157
2,3-dihydro-4-methyl-1*H*-indene	$C_{10}H_{12}$				0.244	0.902
1,2,3,4-tetrahydronaphthalene	$C_{10}H_{12}$					0.073
bicyclopentyl-1,1′-diene	$C_{10}H_{14}$					0.047
bicyclopentyl-1,1′-diene	$C_{10}H_{14}$					0.041
cis-8-ethyl-*exo*-tricyclo[5.2.1.0(2.6)]decane	$C_{12}H_{20}$					0.099
trans-syn-tricyclo[7.3.0.0(2,6)]-8-dodecene	$C_{12}H_{18}$					0.141
1,2,3,6,7,8-hexahydro-*as*-indacene	$C_{12}H_{14}$				0.050	0.188
residue		0.000	0.000	1.591	6.302	13.707

[a] Reactant. [b] Molecular formula.

compounds, such as cyclopentene (boiling temperature 317 K), from vaporizing. The chemical composition of the products was determined by GC/MSD (Agilent 7890A Series GC Custom, 5975C inert MSD Standard Turbo EI) equipped with a HP-5 ms column. In the GC/MSD analysis, if the main peaks in the mass spectrum of the product compound did not match the main peaks in the reference of the Wiley library by more than two peaks, the compound was labeled as residue in Table 1, since its identity could not be accurately determined.

3. Molecular Modeling

Calculations of the decomposition pathway were performed using quantum mechanical calculation. The procedure used to search for the decomposition pathway was as follows: Optimization of molecular structures of reactants and products by minimization of configurational energy (steric energy). Search for reaction intermediate (transient state) and its activation energy from reactant to product. All molecular structures of reactants and products were preliminarily optimized to obtain the minimum energy using the MM3 method[17] of CACHe before that main calculations were performed. The decomposition mechanism of *exo*-THDCP was suggested, which was determined using the optimized structure and calculating the minimization energy. To determine the decomposition pathway, the energy calculation of the intermediate was carried out using the semiempirical PM3 method[18] in the MOFAC (CACHe 7.7)[19] software package. The map reaction function of this program was used to determine the intermediate form (Figure 1).

4. Experimental Results and Discussion

4.1. Thermal Stability of *exo*-THDCP. As shown in Figure 2, the *exo*-THDCP was thermally stable under 603 K but it decomposed at temperatures greater than 683 K. In addition, 72.145% of its composition remained in the liquid phase 10 h after completion of the reaction at 683 K, whereas 97.878% of its composition was in the liquid phase before the reaction. The composition of the other reactants, *endo*-THDCP, adamantane, and *trans*-decalin, only slightly varied compared to their composition before the reaction. The increment rate of composition of *endo*-THDCP was higher than adamantine and *trans*-decalin as the temperature increased. This increase in composition of *endo*-THDCP could be explained by reversible Wagner−Meerwein rearrangement.[20]

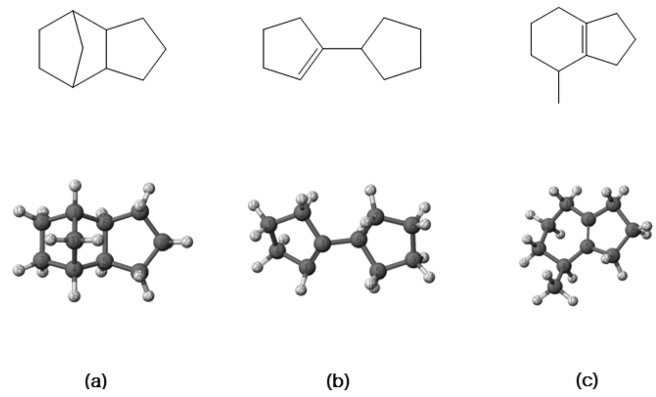

Figure 1. Molecular structure and optimized molecular structure by molecular modeling: (a) *exo*-THDCP; (b) 1-cyclopentylcyclopentene; (c) 4-methyl-2,3,4,5,6,7-hexahydro-1*H*-indene.

C_{10} hydrocarbons only constituted 0.139% of the decomposition product after completion of the reaction at 623 K, as shown in Table 2 and Figure 3. However, as the temperature of the reaction increased, C_{10} hydrocarbons and C_{13}−C_{14} hydrocarbons became the major decomposition products of *exo*-THDCP relative to C_5−C_9 hydrocarbons. These results were different from those reported in previous studies,[1,6−9] where hydrocarbons under C_6 such as cyclopentene, cyclopentadiene, benzene, and toluene were the major decomposition products of *exo*-THDCP.

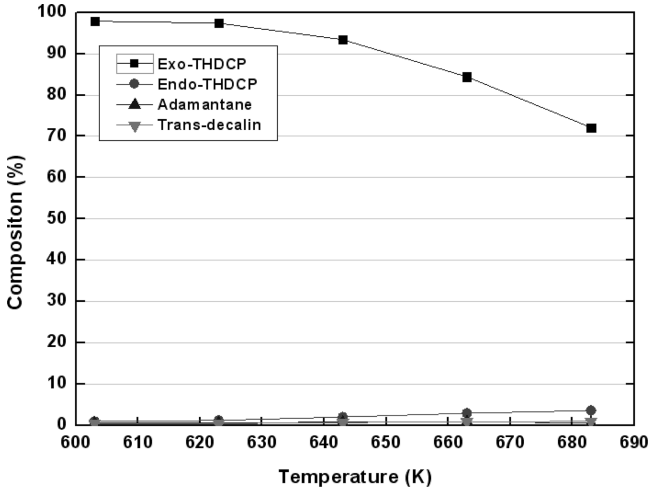

Figure 2. Thermal stability of *exo*-THDCP: variation in the composition of reactants, without products.

Table 2. Distribution of Decomposition Products of *exo*-THDCP Classified by the Number of Carbons, without Reactants

no. of carbons	623 K	643 K	663 K	683 K
5		0.126	0.382	0.594
6		0.000	0.000	0.035
7		0.000	0.049	0.236
8		0.044	0.115	0.265
9		0.000	0.270	0.657
10	0.139	4.897	8.983	13.093
11−12		0.000	0.418	1.596
13−14		1.547	5.385	11.380

In these previous studies, low molecular weight hydrocarbons, except hydrocarbons around C_{10}, were the main products, because the reaction temperature, which is an important parameter of the decomposition of *exo*-THDCP as well as hydrocarbons, was over 773 K.

The structures of C_{10} products were from the split carbon−carbon bond of *exo*-THDCP by β-scission. The relatively high composition of C_{10} products meant that β-scission was more dominant than thermal cracking to low-molecular-weight compounds. Analysis of the mechanism for production of the $C_{13}-C_{14}$ component was difficult because most of them were not determined by GC−MS. The structures of some products specified by GC−MS were triple-ring compounds such as *trans-syn*-tricyclo[7.3.0.0$^{(2,6)}$]-8-dodecene ($C_{12}H_{18}$), 1,2,3,6,7,8-hexahydro-*as*-indacene ($C_{12}H_{14}$), and 1,3-dicyclopentylcyclopentane ($C_{15}H_{16}$). On the basis of these three compounds, it could be

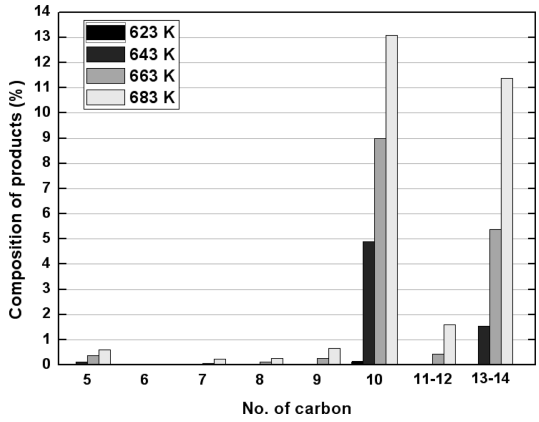

Figure 3. Distribution of decomposition products of *exo*-THDCP classified by the number of carbons, without reactants.

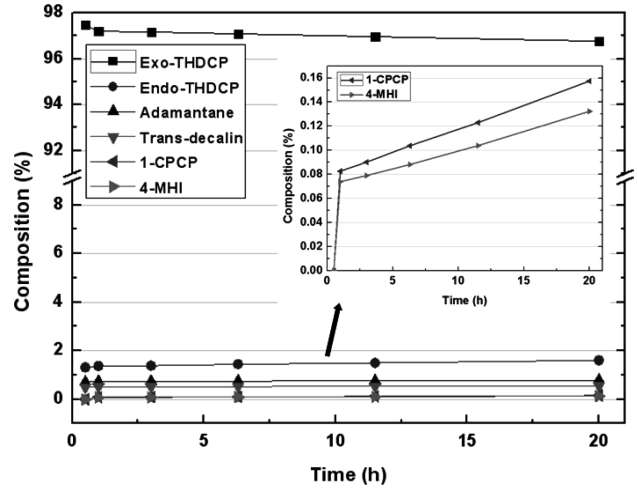

Figure 4. Composition of reactants and products at 623 K.

predicted that radical polymerization occurred after splitting the carbon−carbon bond of *exo*-THDCP by β-scission. It could be assumed that after the radical of *exo*-THDCP was formed by β-scission, radical polymerization was more dominant than thermal cracking to low-molecular-weight compounds such as one-ring compounds (cyclopentene, cyclopentane, ethylcyclopentane, or methylbenzene).

The overall decomposition mechanism of *exo*-THDCP was already schematically demonstrated in several studies.[1,2,6,8,9] Therefore, we focused on analyzing the primary initiation of *exo*-THDCP.

4.2. Primary Initiation of *exo*-THDCP. 1-CPCP and 4-MHI were identified to be the primary initiation products of *exo*-THDCP decomposition at a reaction temperature of 623 K. However, their production pathways from *exo*-THDCP were not specified. In other words, there were two possible decomposition pathways of *exo*-THDCP to 1-CPCP and 4-MHI. The first potential pathway was that both 1-CPCP and 4-MHI were simultaneously decomposed from *exo*-THDCP. The second potential pathway was that one of them was first directly decomposed from *exo*-THDCP and the other was produced from the decomposition of the first product. As shown in Figure 4, 1-CPCP and 4-MHI were simultaneously produced after 1 h at 623 K and the amount of each component increased uniformly as the reaction time increased. These results indicated that they simultaneously and independently decomposed from *exo*-THDCP. Molecular modeling was performed for a more detail analysis and understanding of this process.

5. Molecular Modeling Results

To determine the mechanism by which 1-CPCP and 4-MHI were produced from *exo*-THDCP, we performed molecular modeling by considering intermediate structures and the activation energy of the reaction. In addition, we also performed molecular modeling on adamantane, which was present before and after the reaction, and 2,2-dimethyl-5-methylenebicyclo-[2.2.1]heptane (2D5MBH), which was not present before the reaction but was present after the reaction. This work was conducted to analyze their relatively low composition after the reaction and the calculated energy value was qualitatively analyzed. The decomposition pathway "*exo*-THDCP → 1-CPCP" is presented in Figure 5. The calculated energy values and molecular structure of intermediate for each conformation are

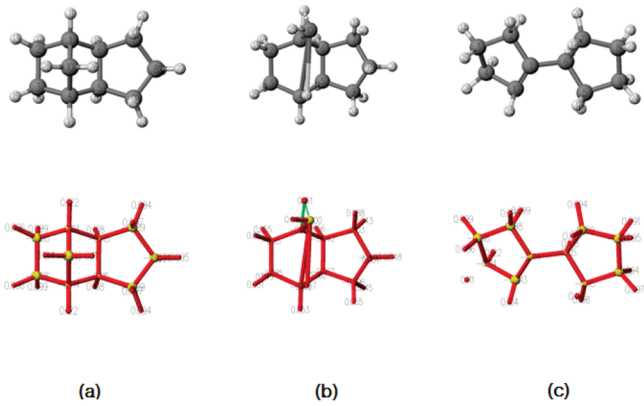

Figure 5. Decomposition mechanism of *exo*-THDCP to 1-CPCP: (a) *exo*-THDCP; (b) intermediate; (c) 1-CPCP. Partial charge: red (positive), yellow (negative). Bond order and bond type: green (0−0.60, weak), red (0.61−1.60, single), yellow (1.61−2.60, double).

Table 3. Energy Variation from Reactant to Product

		configurational energy (kcal/mol)			activation energy
reactant	product	reactant	intermediate	product	(kcal/mol)
exo-THDCP	1-CPCP	32	74	18	42
exo-THDCP	4-MHI	32	82	23	50
1-CPCP	4-MHI	18	115	23	97
4-MHI	1-CPCP	23	117	18	94
exo-THDCP	adamantane	32	187	27	155
exo-THDCP	2D5MBH	32	352	51	320

shown in Table 3 and Figure 6, respectively. The decomposition mechanism from reactant to product was expressed as "reactant → product".

5.1. *exo*-THDCP → 1-CPCP. Figure 5 shows the structural decomposition mechanism of *exo*-THDCP (reactant) to 1-CPCP (product). When the formation of an intermediate was considered, the bond length between C(10) and H(16) of *exo*-THDCP became longer and weak enough to be scissile. In addition, the bond between C(1) and H(16) became longer and a bond between C(1) and C(10) was generated. The negative charge of C(10) increased, and the bond between C(10) and C(1) was expected to be a double bond. Through this sequence, *exo*-THDCP could be decomposed to 1-CPCP. Therefore, the intermediate specified in Figure 5 could be used to explain the decomposition mechanism of *exo*-THDCP to 1-CPCP. The activation energy from *exo*-THDCP to 1-CPCP was calculated to be 41 kcal/mol, which explained why the production of 1-CPCP was relatively high during the decomposition of *exo*-THDCP.

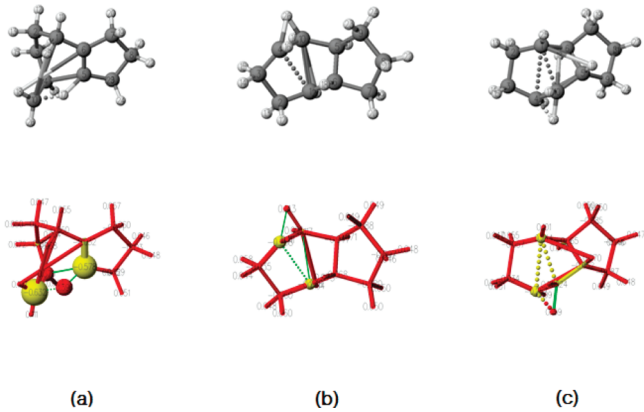

Figure 6. Intermediates for each pathway: (a) *exo*-THDCP → 4-MHI; (b) 1-CPCP → 4-MHI; (c) 4-MHI → 1-CPCP.

5.2. *exo*-THDCP → 4-MHI. Figure 6a shows the molecular structure of intermediate for decomposition mechanism of *exo*-THDCP to 4-MHI, which was the other primary initiation product of *exo*-THDCP, whose composition was 0.058% at a reaction temperature of 623 K. When the formation of the intermediate was considered, it was expected that the bond length between C(10) and H(25), C(1) and C(1), C(5) and H(17), and C(6) and H(18) became longer and weak enough to be scissile. On the other hand, the negative charge of C(5) drastically increased and the negative charge of the bond between C(5) and C(6) also increased enough to become a double bond because the strong negative charge was proportional to the bond order. Therefore, the intermediate specified in Figure 6a could be used to explain the decomposition mechanism of *exo*-THDCP to 1-CPCP. As shown in Table 3, the activation energy from *exo*-THDCP to 4-MHI was 50 kcal/mol. This result explained why more 1-CPCP was produced than 4-MHI during the decomposition of *exo*-THDCP.

5.3. *exo*-THDCP → 1-CPCP → 4-MHI. In the previous section, molecular modeling was used to determine the primary initiation mechanism of *exo*-THDCP to either 1-CPCP or 4-MHI. However, these mechanisms could not be used to determine whether both 1-CPCP and 4-MHI were directly produced from the decomposition of *exo*-THDCP. Namely, if the activation energy for conversion of 1-CPCP to 4-MHI was lower than 50 kcal/mol, which was the activation energy required to produce 4MHI from *exo*-THDCP, 4-MHI could be produced from 1-CPCP after 1-CPCP was produced from *exo*-THDCP. Therefore, we investigated the mechanism of producing 4-MHI from 1-CPCP after it was produced from *exo*-THDCP. The production of 1-CPCP from *exo*-THDCP was not examined in this section, since it was described in the previous section. Figure 6b shows the intermediate determined by molecular modeling for the production of 4-MHI from 1-CPCP. The activation energy for this reaction was calculated to be 96 kcal/mol, which was 46 kcal/mol higher than the activation energy of producing 4-MHI directly from the decomposition of *exo*-THDCP. Therefore, it is likely that 4-MHI is directly produced from *exo*-THDCP rather than being produced from 1-CPCP.

5.4. *exo*-THDCP → 4-MHI → 1-CPCP. In light of the above results, we also examined whether 1-CPCP could be produced from 4-MHI. The activation energy of producing 1-CPCP from *exo*-THDCP was 41 kcal/mol. Therefore, if the activation energy for producing 1-CPCP from 4-MHI is less than 41 kcal/mol, it is likely that 1-CPCP is not produced from *exo*-THDCP. However, the molecular modeling result indicated that the activation energy of producing 1-CPCP from 4-MHI was 93 kcal/mol, as shown Table 3. On the basis of these results, 1-CPCP is most likely directly produced from the decomposition of *exo*-THDCP rather than through the 4-MHI produced from *exo*-THDCP with respect to activation energy. The intermediate from 4-MHI to 1-CPCP is shown in Figure 6c. Figure 7 shows that energy variation in each reaction pathway of 4-MHI from *exo*-THDCP and 1-CPCP from *exo*-THDCP.

5.5. *exo*-THDCP → Adamantane, *exo*-THDCP → 2D5MBH. There were lots of compounds produced in very low quantities at a reaction temperature of 683 K. Therefore, we investigated the activation energy required to produce these compounds to determine if these values were related to their low levels of production. First, we investigated adamantane, whose composition was almost constant both before and after the reaction. It was previously proposed that adamantane was produced from *exo*-THDCP or *endo*-THDCP through a step mechanism.[20] However, the activation energy of producing

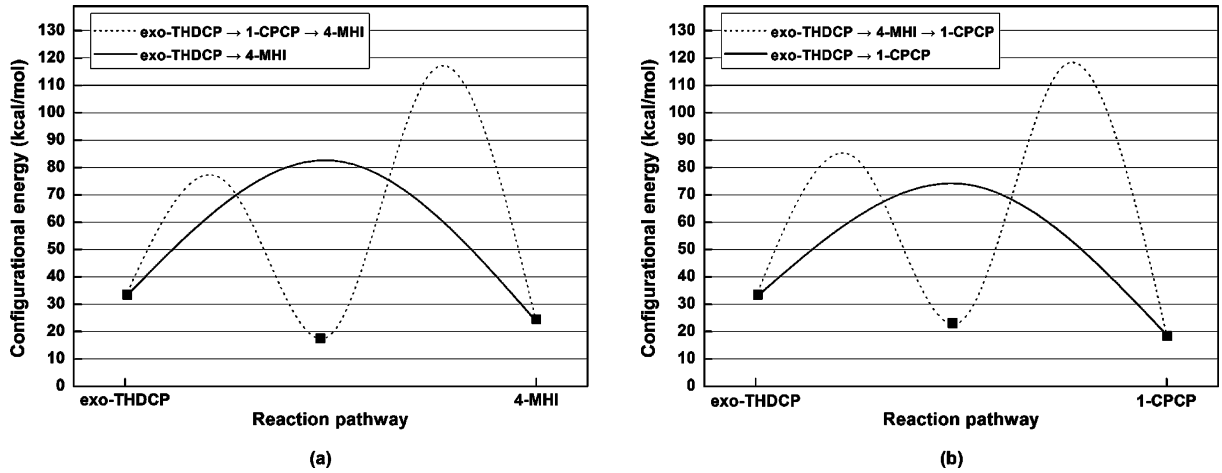

Figure 7. Energy variation and reaction pathway: (a) 4-MHI from *exo*-THDCP; (b) 1-CPCP from *exo*-THDCP.

adamantane from *exo*-THDCP was investigated by molecular modeling without considering the entire step mechanism. The activation energy producing adamantane from *exo*-THDCP was determined to be 155 kcal/mol. This value was 100 kcal/mol higher than the activation energy required to produce either 1-CPCP or 4-MHI. Thus, the production of adamantane from *exo*-THDCP was expected to be qualitatively very low due to the high activation energy of the reaction. Second, we investigated the production of 2D5MBH, which did not exist before the reaction but was present after the reaction at a reaction temperature of 643 K. According to the molecular modeling results, the activation energy of 2D5MBH from *exo*-THDCP was 319 kcal/mol. Thus, production of 2D5MBH from *exo*-THDCP would be qualitatively lower than production of adamantane with respect to the activation energy, except when the decomposition of 2D5MBH to other low-molecular-weight compounds was considered.

6. Comparison between Experimental and Molecular Modeling

A comparison between the activation energy of the primary decomposition products of *exo*-THDCP by molecular modeling and their experimentally determined composition is available in Tables 1 and 3. At 603 K, the composition of 1-CPCP, 4-MHI, and 2D5MBH was 0%. The change in composition of adamantane was also 0%, since the composition of adamantane both before and after the reaction was 0.61%. At 623 K, 1-CPCP and 4-MHI were produced at the same time and constantly increased as a function of time. In these experiments, more 1-CPCP was produced than 4-MHI, which corresponded with the molecular modeling results; the activation energy for the production of 1-CPCP was lower than that of 4-MHI. Also, at reaction temperatures ranging from 643 to 683 K, it was experimentally shown that the composition of 1-CPCP, whose activation energy was lower than that of 4MHI, was higher than 4-MHI, although the composition of the products could not be directly compared to the calculated activation energy because the decomposition of these products to other compounds was not considered.

Adamantane is most likely produced from either *exo*-THDCP or other compounds and it is likely decomposed to other compounds. However, it has been shown that adamantane decomposes at temperatures greater than 873 K.[21] Therefore, in the reaction conditions of this study, adamantane could be only produced from the decomposition of *exo*-THDCP. The composition of adamantane, which has an activation energy of 155 kcal/mol, increased by 0.035% at 623 K, 0.257% at 663 K, and 0.269% at 683 K. These results showed that the production of a compound with high activation energy was lower than those with low activation energy, although we only considered production of these compounds from *exo*-THDCP and not other compounds and did not considered decomposition of these compounds to other low-molecular-weight molecules.

7. Conclusion

exo-THDCP was thermally decomposed to test its thermal stability in a batch-type reactor after eliminating the catalytic effects of the metal. *exo*-THDCP was decomposed at temperatures above 623 K, and it became more decomposed as the reaction temperature increased. 1-CPCP and 4-MHI were determined to be the primary decomposition products of *exo*-THDCP. Although C_5 to C_{14} hydrocarbons were also produced as decomposition products of *exo*-THDCP when the reaction temperature was increased, C_{10} hydrocarbons were the major products. Molecular modeling was performed on *exo*-THDCP to investigate the decomposition pathway and activation energy of the products produced through the decomposition of *exo*-THDCP. With molecular modeling, intermediates from *exo*-THDCP to 1-CPCP and 4-MHI were proposed and the experimental results were found to correspond with the molecular modeling results in terms of relating composition (experimental) to activation energy (MM).

Supporting Information Available: Details of the process flow diagram. This material is available free of charge via the Internet at http://pubs.acs.org.

Literature Cited

(1) Davidson, D. F.; Horning, D. C.; Oehlschlaeger, M. A.; Hanson, R. K. THE DECOMPOSITION PRODUCTS OF JP-10. In *Proceedings of the 37th AIAA/ASME/SAE/ASEE Joint Propulsion Conference and Exhibit*, Salt Lake City, UT, July 8−11, 2001; AIAA 01-3707.

(2) Li, S. C.; Varatharajan, B.; Williams, F. A. Chemistry of JP-10 Ignition. *AIAA J.* **2001**, *39*, 2351.

(3) Wohlwend, K.; Maurice, L. Q.; Edwards, T.; Striebich, R. C.; Vangsness, M.; Hill, A. S. Thermal Stability of Energetic Hydrocarbon Fuels for Use in Combined Cycle Engines. *J. Propul. Power* **2001**, *17*, 1258.

(4) Cooper, M.; Shepherd, J. E. Experiments Studying Thermal Cracking, Catalytic Cracking, and Pre-Mixed Partial Oxidation of JP-10. In *Proceedings of the 39th AIAA/ASME/SAE/ASEE Joint Propulsion Conference and Exhibit*, Huntsville, AL, July 20−23, 2003; AIAA 2003-4687.

(5) Striebich, R. C.; Lawrence, J. Thermal decomposition of high-energy density materials at high pressure and temperature. *J. Anal. Appl. Pyrolysis* **2003**, *70*, 339.

(6) Herbinet, O.; Sirjean, B.; Bounaceur, R.; Fournet, R.; Battin-Leclerc, F.; Scacchi, G.; Marquaire, P.-M. Primary mechanism of the thermal decomposition of tricyclodecane. *J. Phys. Chem. A* **2006**, *110*, 11298.

(7) Nageswara Rao, P.; Kunzru, D. Thermal cracking of JP-10: Kinetics and product distribution. *J. Anal. Appl. Pyrolysis* **2006**, *76*, 154.

(8) Nakra, S.; Green, R. J.; Anderson, S. L. Thermal decomposition of JP-10 studied by micro-flowtube pyrolysis-mass spectrometry. *Combust. Flame* **2006**, *144*, 662.

(9) Xing, Y.; Fang, W.; Xie, W.; Guo, Y.; Lin, R. Thermal Cracking of JP-10 under Pressure. *Ind. Eng. Chem. Res.* **2008**, *47*, 10034.

(10) Chenoweth, K.; van Duin, A. C. T.; Dasgupta, S.; Goddard, W. A., III. Initiation Mechanisms and Kinetics of Pyrolysis and Combustion of JP-10 Hydrocarbon Jet Fuel. *J. Phys. Chem. A* **2009**, *113*, 1740.

(11) Kwon, C.; Jeong, J.; Kang, J. Molecular modeling and experimental verification of lipase-catalyzed enantioselective esterification of racemic naproxen in supercritical carbon dioxide. *Korean J. Chem. Eng.* **2009**, *26*, 214.

(12) Kwon, C. H. Molecular Modeling and its Experimental Verification for the Catalytic Mechanism of Candida antarctica Lipase B. *J. Microbiol. Biotechnol.* **2007**, *17*, 1098.

(13) Simpson, T. W.; Peplinski, J.; Koch, P. N.; Allen, J. K. Metamodels for Computer-Based Engineering Design: Survey and Recommendations. *Eng. Comput.* **2001**, *17*, 129.

(14) Leonor, S.; Michael, L. K. Computer simulation studies of model biological membranes. *Acc. Chem. Res.* **2002**, *35*, 482.

(15) Arlene, R.; Mark, M.; Robert, A. C.; Karl, H.; Carl, P. D.; William, F. D. Complementarity of Combinatorial Chemistry and Structure-Based Ligand Design: Application to the Discovery of Novel Inhibitors of Matrix Metalloproteinases. *J. Am. Chem. Soc.* **1996**, *118*, 10337.

(16) Osmont, Antoine; Goalp, Iskender; Catoire, Laurent. Evaluating Missile Fuels. *Propellants, Explos., Pyrotech.* **2006**, *31*, 343.

(17) Allinger, N. L.; Li, F.; Yan, L. Molecular Mechanics. The MM3 Force Field for Alkenes. *J. Comput. Chem.* **1990**, *11*, 848.

(18) Stewart, J. P. Optimization of parameters for semiempirical methods II. Applications. *J. Comput. Chem.* **1989**, *10*, 221.

(19) CACHe Workspace Ver. 7.7, Fujitsu.

(20) Schleyer, P. v. R.; Donaldson, M. M. The Relative Stability of Bridged Hydrocarbons. II. endo- and exo-Trimethylenenorbornane. The Formation of Adamantane. *J. Am. Chem. Soc.* **1960**, *82*, 4645.

(21) Kazanskii, B. A. The pyrolysis of adamantine. *Russ. Chem. Bull.* **1968**, *17*, 2506.

Received for review January 12, 2010
Revised manuscript received July 23, 2010
Accepted August 4, 2010

IE100065M